Journal of Mathematical Chemistry Vol. 33, No. 1, January 2003 (© 2003)

Shell structures in molecular orbital energy diagrams for "small" fullerene cages: Free-electron versus generator orbital models

Gordon J. Miller and John G. Verkade

Department of Chemistry, Iowa State University, Ames, IA 50011, USA

Received 1 March 2002

The nearly spherical nature of small fullerene cages C_N ($N < 70$) suggests that their π molecular orbital (MO) energy diagrams should show a shell structure. Although group theoretical analysis of the Hückel-type energies for icosahedral and other highly symmetric cages confirms this assumption, this has not been established for fullerene cages in general. This work presents a simple computational algorithm based upon the canonical orthogonalization of generator orbitals (GOs) to analyze the π-MO energy diagrams for any fullerene cage C_N, and demonstrates the validity of a shell structure in these diagrams. Results are compared to simple central force (spherical) models for the calculations of π-MO energies in fullerene cages. The GO approach provides a ready assignment of the π-MOs to individual spherical harmonics and allows valuable interpretations of various physical phenomena.

KEY WORDS: Hückel MO theory, generator orbitals, spherical harmonics, fullerenes

1. Introduction

The chemistry of carbon clusters exploded with the discovery and eventual characterization of buckminsterfullerene (C_{60}) in the 1980s [1–4], and continues to grow because macroscopic quantities of C_{60} are available. This beautifully symmetric molecule is "breathing fresh life into some old, well-established methods and principles" [5]. However, to date, very few other "fullerenes" have been isolated and structurally characterized from experiments, e.g., C_{70} [6,7] and solid C_{36} [8]. Theoretical calculations and ^{13}C nuclear magnetic resonance spectroscopy play a huge role in elucidating the structures of other fullerenes ranging from C_{20} to C_{102} and beyond [9–11].

The general feature of fullerene structures is three-bonded carbon atoms with pentagonal and hexagonal faces to keep C–C–C bond angles around 109—120° (fullerenes are trivalent, nonalternant graphs). According to Euler's relationship between vertices, edges and faces of convex polyhedra [12], the numbers of pentagonal and hexagonal faces, respectively, must be 12 and $N/2 - 10$ for a C_N fullerene. The ground state structures of fullerenes below C_{102}, as determined by tight-binding molecular-dynamics total energy optimization [9–11], prefer cages that separate the pentagonal rings as far

0259-9791/03/0100-0055/0

apart as possible (which is part of the "pentagon rule" for fullerenes) while only a few cages prefer high symmetry, e.g., C_{60} and C_{70}. In fact, C_{60} is the first possible "isolated pentagon" fullerene.

Numerous calculations of the electronic structure of fullerenes exist [13–18], with much effort devoted to elucidating the chemistry and properties of C_{60} and finding simple rules for the stability of high nuclearity fullerene cages [19,20]. Useful qualitative information about the electronic structures of these systems has been obtained from simple Hückel theory, which revealed the $60 + 6k$ leapfrog rule for closed π-shell fullerenes [21]. For qualitative molecular orbital (MO) methods, such as Hückel theory, ordering of molecular orbital energies is frequently achieved by "node counting" [22,23]. Along these lines, one of us has developed a pictorial method for constructing the MOs for a wide assortment of discrete molecular, polymeric [24], and solid state structures [25] – the "generator orbital" (GO) method [23]. The central idea of this approach is that each MO of a molecule has symmetry characteristics of a specific atomic orbital located at the molecular center, called a generator orbital (GO). Therefore, the nodal properties of any symmetry-adapted linear combination of atomic orbitals (SALCs) are patterned after the nodal surfaces of the corresponding GO. The large number of examples successfully described by this method attests to its qualitative reliability [23].

In this article we explore the application of the GO approach via a simple computational algorithm to the interpretation of π-MO energy diagrams of small fullerene cages, i.e., C_N fullerenes with $N \leqslant 70$. We chose structures based on the results of [9] since few of these structures have been experimentally characterized. The article is organized as follows: (1) initial comments on the strengths and limitations of two quantitatively simple methods to estimate a pattern of MO energies for fullerenes, based on the central force approximation; (2) development of the computational algorithm to relate qualitatively useful GOs to Hückel eigenfunctions and their eigenvalues for fullerene-related cages; and (3) examples of results for small nuclearity C_N cages ($20 \leqslant N \leqslant 70$).

2. Simple methods for MO energies of fullerenes

The patterns of valence MO energies for C_N fullerene cages are complex because $4N$ valence atomic orbitals (VAOs) will give $4N$ valence MOs. But, since much of the chemical and physical properties of fullerenes are governed by the occupied and unoccupied states near the HOMO–LUMO gap, many methods simplify the total pattern of MOs by focusing just on the "surface π-MOs" (see figure 1), which are simply N radial $2p$ orbitals (we can call them $2p_z$ VAOs by placing a local z-axis at each carbon atom). The remaining $3N$ valence orbitals separate into $3N/2$ σ-bonding and $3N/2$ σ-antibonding sp^2 hybrid orbitals. The $2p_z$ VAO is also perpendicular to the sp^2 hybrid VAO set at each carbon atom, and overlaps with neighboring $2p_z$ VAOs according to the expression $\beta = \cos^2\omega\beta_\pi + \sin^2\omega\beta_\sigma$ [26], where ω is the angle subtended by the C–C bond (edge) of the fullerene cage (see figure 2). There is a σ-overlap component to the orbital interactions among the surface π-MOs, but the relative contribution is small.

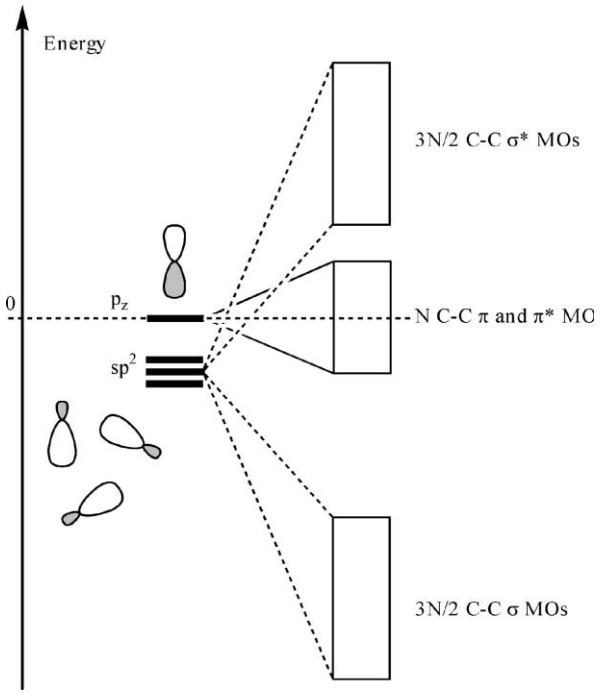

Figure 1. Simple scheme for the distribution of σ- and π-MOs in fullerenes. This picture qualitatively justifies the attention only to the π-MOs.

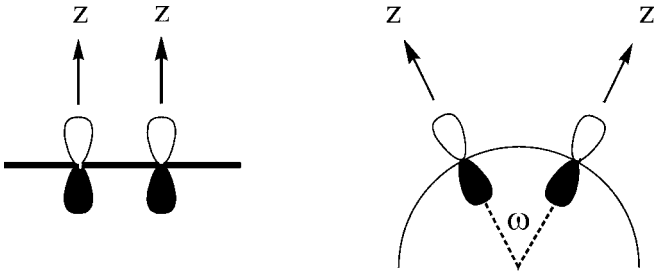

Figure 2. (Left) True π overlap of a pair of $2p_z$ VAOs. (Right) The mostly π overlap of a pair of $2p_z$ VAOs on the surface of a fullerene cage.

Furthermore, the π contribution to the total overlap increases as the size of the cage increases, since the angle ω decreases with increasing size of the cage. We will focus only on the N surface π-MOs derived from these $2p_z$ VAOs.

Since fullerene cages are nearly spherical,[1] the π-MO energy diagrams are expected to show a shell structure, which can be quickly obtained by using models of

[1] Haddon questions whether C_{60} should be described as a "sphere" or as a "polyhedron" [27]. He ultimately concludes that C_{60} (and other fullerenes as well) are best modeled as polyhedra, with his strongest argument coming from the diamagnetic properties of C_{60}.

electronic structure based on the central force approximation. For these structures, two important models would be appropriate:

(a) *"Free electrons" confined to a spherical shell* [28]. If the three-dimensional symmetry of fullerene molecules is approximated as a sphere, then electrons occupying the surface π-MOs are distributed over the entire spherical shell of radius R and move in a constant potential (there are no distinct positions for the nuclei in this model). Therefore, the electronic energies involve entirely kinetic energy with the sphere radius (R) controlling the difference between energy levels. The expression for these free electron energy levels $E_l^{(\mathrm{FE})}$ corresponds to the three-dimensional rigid rotor [28]:

$$E_l^{(\mathrm{FE})} = A\frac{l(l+1)}{R^2}, \tag{1}$$

where $A = (\hbar^2/2m) = 3.8101$ eV·Å^2 and $l = 0, 1, 2, 3, \ldots$. Equation (1) is a quadratic relationship between energy and quantum number and shows a curvature of A/R^2, which means that the curvature decreases as the size of the cage increases. The corresponding eigenfunctions $\psi_{lm}^{(\mathrm{FE})}(\theta, \phi)$ are the spherical harmonics $Y_l^m(\theta, \phi)$ (i.e., s, p, d, f, etc. orbitals), so the degeneracy associated with each energy level is $2l + 1$. Therefore, each shell can have a maximum of $2(2l + 1)$ electrons. According to this model, "magic electron counts" for fullerenes would be 32, 50, 72, etc., which means that the neutral molecules C_{32}, C_{50}, C_{72}, etc. would have closed shell electronic configurations and represent stable molecules. If this model is applied to C_{60} with 60 π electrons, all levels are filled up to the $l = 5$ level, which is partially filled with 10 unpaired electrons. Ball [28] has shown that this model accounts numerically for three observed electronic absorptions in C_{60}, although one of the assigned transitions is between two excited states in this simple model. However, this model is inconsistent with the diamagnetic behavior of C_{60}, which requires no unpaired electrons.

(b) *Electrons moving in a spherical potential of N atoms on a spherical surface*. In this model, the cage molecule is treated as a spherical shell (radius R) of positive charge NZ and the electrons move throughout all space. Inside the cage, the potential for the electrons is constant, while outside the cage the potential follows Coulomb's law: $V(r) = -(NZe)^2/(r - R)$. Wannier solved this problem and obtained the following approximation to the energy levels [29–31]:

$$E_{nl}^{(\mathrm{W})} \approx -\frac{(NZ)^2}{[n - (2l+1)/4 + (2NZR)^{1/2}/\pi]^2} \tag{2}$$

where $n = 1, 2, 3, \ldots$, and for each n, $l = 0, 1, 2, \ldots, n - 1$. The corresponding eigenfunctions $\psi_{nlm}^{(\mathrm{W})}(r, \theta, \phi)$ (W = "Wannier") are atomic-like functions involving the product of a radial function (spherical Bessel functions) and the spherical harmonics, $j_{nl}(r)Y_l^m(\theta, \phi)$. There is a shell structure for the energy

levels, whose energies increase as $(1s) < (2p) < (2s, 3d) < (3p, 4f) < (3s, 4d, 5g) < (4p, 5f, 6h) < \cdots$. Therefore, for C_{60}, the 60 π electrons will fill orbitals up to the $(3p, 4f)$ shell and leave 20 electrons to fill the 15 orbitals in the $(3s, 4d, 5g)$ shell, which produces 10 unpaired electrons (just as in the free electron model). This model has been discussed by Hoffmann [31] as an approximation to finding MO energies for polyhedral molecules, e.g., boranes and carboranes, but it has not been applied to fullerenes.

These two methods treat fullerene cages as spherical molecules, so that the patterns of energy levels show a shell structure and have orbital degeneracies that exceed three except for the two lowest energy levels. Both methods predict unpaired electrons for buckminsterfullerene, which contradicts its diamagnetic behavior. Although group theoretical methods can show how each shell will separate into levels appropriate for the point group of the molecule, without some type of calculation there exists no convenient method for identifying the sequence of π-MO energies. For high symmetry cages, analytical methods have been developed to give the Hückel energy levels [15,19]. In the following sections, we utilize the GO method to characterize Hückel energy levels and demonstrate that there is a shell structure in the pattern of MO energies.

3. The generator orbital approach: Qualitative aspects

In the GO method the series of atomic orbitals placed at the geometrical center of the molecule in question (called GOs) is used to construct qualitative representations of the MOs for the molecule [23]. In general, these GOs have radial, conical and planar nodes. A systematic, pictorial approach to constructing and visualizing the nodes of any atomic orbital (GO) is given elsewhere [23]. Since the distribution of electron density in fullerene cages is confined mostly to a spherical shell, only GOs with conical and/or planar nodes are used, i.e., the spherical harmonics $1s$, $2p$, $3d$, $4f$, $5g$, etc. Since the spherical harmonics are identified by the quantum numbers l and m, the number of planar nodes is $|m|$ and the number of conical nodes is $l - |m|$. Furthermore, the nodal surfaces of each GO will pass through edges (bonds) and vertices (atoms), which will depend on the orientation of the molecule with respect to the coordinate axes. As more nodes of these GOs intersect the edges of fullerene cages, the antibonding character of the corresponding orbital increases. Since there are N $2p_z$ VAOs in the C_N cage, we must generate N GOs that correspond to the N π-MOs for the fullerene molecule. We can estimate the highest order shell[2] of GOs (L) that will generate all possible π-MOs for the C_N cage: ideally, L is the smallest integer that satisfies the inequality $N \leqslant \sum_{l=0}^{L}(2l + 1) = (L + 1)^2$ (note: the same algorithm will identify the highest occupied shell in the free-electron model described in the previous section). In other words, L is the smallest integer that is greater than or equal to $\sqrt{N} - 1$. For example, in buckminsterfullerene, $N = 60$ and $L = 7$. However, one often has to include higher

[2] We refer to *shell* with respect to the quantum number l in the spherical harmonics functions $Y_l^m(\theta, \phi)$.

order GOs than the L shell due to the possibility of linear dependency in the set of GOs, which is related to the problem of repetitions raised by Redmond et al. in their node-counting treatment of icosahedral carbon cages [19]. Including GOs from higher shells, however, will not increase the total number of GOs: the number of GOs needed must equal the number of MOs in the molecule. One other reason for including higher order GOs arises if the nodes of a GO pass through every atomic position (a *null* GO). We have not observed *null* GOs for fullerene cages, but it is does occur for small borane and carborane deltahedra [23].

Including higher order GOs, however, does create a complication in the final analysis of MOs because each MO will be a linear combination of GOs to create a mutually orthogonal set of orbitals: the set of basis functions we use is *overdetermined*, i.e., the order of the basis exceeds the order of the complete MO diagram. In the spirit of the original GO approach and to simplify the final assignment of MOs to GOs, our computational algorithm evaluates an incomplete set of GOs, i.e., the order of the set of GOs is less than the number of MOs needed for the complete structure. At this stage, the calculated Hückel energy values for this set of GOs does not give complete agreement with the true Hückel values. Then, we include the complete set of GOs to achieve complete agreement. This analysis allows a measure of the extent of hybridization with higher order GOs and provides a means to develop a quick "pictorial" representation of the MO. We demonstrate this concept in some of the subsequent examples.

4. The generator orbital approach: Quantitative aspects

The original goal of the GO method was to construct qualitative MOs for a chemical structure by drawing one GO after another and sketching the effects on the coefficients of each VAO in the LCAO expansion. For the π-MOs of fullerene cages, this procedure is tedious and unnecessary: the spherical harmonics and the nearly spherical shell structure of these cages enable us to program a computer to do this for us. Before describing this algorithm, we note that the GO approach involves creating approximate ("pictorial") MOs to estimate MO energies for the qualitative construction of a MO energy diagram. The typical computational pathway utilizes the LCAO approximation to create a Hamiltonian matrix that is diagonalized to obtain the MO energy levels and the corresponding wavefunctions. In our computer algorithm using the GO method, the GOs constructed an initial set of nonorthogonal (but normalized) functions $\varphi_k(\mathrm{GO})$ for all $k \leqslant (L+1)^2$. We then performed canonical orthogonalization of the $\varphi_k(\mathrm{GO})$ to extract orthonormal orbitals, $\psi_\nu(\mathrm{GO})$, that will transform according to the irreducible representations of the point group of the molecule in question. Linear dependencies among various GOs are recognized at this stage. The set of orthonormal orbitals $\psi_\nu(\mathrm{GO})$ is then used as the basis for a calculation of Hückel MO energies and allows direct computational analysis of the contributions from each GO (i.e., spherical harmonic) to each Hückel MO. Note that this approach does not "replace" the traditional LCAO method for the calculation of MO energies. However, due to numerous accidental degeneracies that arise from the Hückel Hamiltonian with constant overlap integrals (these

degeneracies obviously occur because the group of the graph represented by the Hückel adjacency matrix exceeds the point group of the molecule), this algorithm provides a simple, transparent method for decomposing the MO energy diagram into projections of spherical harmonic-type functions. In the examples discussed in the next section, we point out advantages of this analysis.

The $(L+1)^2$ GO functions for a C_N cage, $\varphi_k(\mathrm{GO})$, are constructed as LCAOs

$$\varphi_k(\mathrm{GO}) = \sum_{j=1}^{N} C_{kj}\chi_j, \tag{3}$$

where χ_j represents a carbon $2p_z$ VAO at the position (x_i, y_i, z_i) in the cage, and the coefficient C_{kj} is the value of the real-form spherical harmonic [32] at those coordinates, i.e., $C_{kj} = \mathrm{Re}(Y_l^m(x_j, y_j, z_j))$, because the actual MOs are real functions. The coefficients are scaled to normalize the functions $\varphi_k(\mathrm{GO})$. Since these functions are vectors in an N-dimensional space, they are linear dependent and there will exist, at least, $[(L+1)^2 - N]$ linear dependency relations between them.

To perform canonical orthogonalization of these nonorthogonal GOs, we need the overlap matrix between $\varphi_k(\mathrm{GO})$'s, which is given by

$$S_{kk'} = \langle \varphi_k(\mathrm{GO}) | \varphi_{k'}(\mathrm{GO}) \rangle = \sum_{i=1}^{N}\sum_{j=1}^{N} C_{ki}C_{k'j}\langle \chi_i | \chi_j \rangle = \sum_{j=1}^{N} C_{kj}C_{k'j}, \tag{4}$$

where we have used the Hückel overlap matrix between atomic orbitals, i.e., $\langle \chi_i | \chi_j \rangle = \delta_{ij}$ (i.e., $\mathbf{S} = \mathbf{C}^{\dagger}\mathbf{X}\mathbf{C}$, where $\mathbf{X} = \mathbf{I}$). The eigenvalues of the overlap matrix are $\{\lambda_\nu\}$ and the eigenvectors are

$$\psi'_\nu = \sum_{k}^{(L+1)^2} T_{k\nu}\varphi_k(\mathrm{GO}). \tag{5}$$

Because of the linear dependencies among $\{\varphi_k(\mathrm{GO})\}$, $[(L+1)^2 - N]$, eigenvalues of this overlap matrix are identically 0. We can, therefore, order the eigenvalues of $\mathbf{S}$ by decreasing magnitude, which assigns the zero eigenvalues to $\lambda_{N+1}, \ldots, \lambda_{(L+1)^2}$. Also, since the overlap matrix, by construction, embodies the geometry and symmetry of the C_N cage, the eigenvectors span irreducible representations of the molecular invariance group. The eigenvectors in this form are mutually orthogonal but not normalized: the overlap integrals between them will be

$$\langle \psi'_\mu | \psi'_\nu \rangle = \sum_{k'}^{(L+1)^2}\sum_{k}^{(L+1)^2} T_{k'\mu}T_{k\nu}S_{k'k} = \lambda_\nu\delta_{\mu\nu}. \tag{6}$$

Equation (6) has two implications: (i) for $\nu > N$, $\langle\psi'_\nu|\psi'_\nu\rangle = 0$, which means that the equations,

$$\psi'_\nu = \sum_k^{(L+1)^2} T_{k\nu}\varphi_k(\mathrm{GO}) = 0 \quad \text{for } \nu = N+1, \ldots, (L+1)^2, \tag{7}$$

are the $[(L+1)^2 - N]$ linear dependency relationships among $\{\varphi_k(\mathrm{GO})\}$; and (ii) for $\nu \leqslant N$, $\langle\psi'_\nu|\psi'_\nu\rangle = \lambda_\nu$, from which we can calculate the orthonormal orbitals constructed from the GOs

$$\psi_\nu = (\lambda_\nu)^{-1/2} \sum_k^{(L+1)^2} T_{k\nu}\varphi_k(\mathrm{GO}) = \sum_k^{(L+1)^2} a_{k\nu}\varphi_k(\mathrm{GO}) = \sum_k^{(L+1)^2}\sum_{j=1}^{N} a_{k\nu}C_{kj}\chi_j, \tag{8}$$

which is represented as both a linear combination of GOs (LCGO) as well as AOs (LCAO). At this point, the Hückel Hamiltonian matrix [26] is constructed and diagonalized using this set of orthonormal functions. Note: for the calculation, we have used the assignment of matrix elements between AOs:

$$\langle\chi_i|H|\chi_j\rangle = \begin{cases} \alpha_i = \alpha = 0, & \text{for } i = j, \\ \beta_{ij} = \beta = -1, & \text{for } i, j \text{ nearest neighbors}, \\ 0, & \text{otherwise}. \end{cases} \tag{9}$$

It is well known that the Hückel method is a drastic approximation to achieve quantitative MO energy diagrams, but the method does reproduce numerous energetic and structural relationships when symmetry arguments are important, which is often the case for fullerenes [13–18].

The final eigenfunctions specified with respect to the GOs are

$$\Psi_n = \sum_{\nu=1}^{N} b_{n\nu}\psi_\nu = \sum_{\nu=1}^{N}\sum_k^{(L+1)^2} a_{k\nu}b_{n\nu}\varphi_k(\mathrm{GO}) \tag{10}$$

corresponding to the eigenvalue E_n. Analysis of each MO involves determining the fraction of each GO that contributes to the MO Ψ_n, $f_n(\varphi_k(\mathrm{GO}))$:

$$f_n\big(\varphi_k(\mathrm{GO})\big) = \sum_{\mu=1}^{N}\sum_{\nu=1}^{N} b_{n\mu}b_{n\nu}\sum_{k'}^{(L+1)^2} a_{k'\mu}a_{k\nu}S_{k'k}, \tag{11}$$

which is a complicated summation of products because $\{\varphi_k(\mathrm{GO})\}$ is not an orthogonal set of functions. We can also analyze the significance of a particular GO to the total MO energy diagram by evaluating the following summation over all N MOs:

$$f_{\mathrm{TOT}}\big(\varphi_k(\mathrm{GO})\big) = \sum_{n=1}^{N} f_n\big(\varphi_k(\mathrm{GO})\big). \tag{12}$$

Table 1
Contributions from GOs to the π-MO energy diagrams for selected fullerenes. The number of π-MOs equals $(L+1)^2$ − number of dependency relations. For each example, two values of L are listed to give both underdetermined and overdetermined results.

	C_{20} ($\mathcal{I}_h$)		C_{28} ($\mathcal{T}_d$)		C_{36} ($\mathcal{D}_{6h}$)		C_{50} ($\mathcal{D}_{5h}$)		C_{60} ($\mathcal{I}_h$)		C_{70} ($\mathcal{D}_{5h}$)	
L	3	4	4	5	5	6	6	7	7	8	8	9
1s (1)	1.00	1.00	1.00	1.00	1.00	1.00	1.00	1.00	1.00	1.00	1.00	1.00
2p (3)	3.00	3.00	3.00	2.98	2.96	2.96	3.00	2.98	2.99	2.99	2.99	2.98
3d (5)	5.00	4.22	5.00	4.58	5.00	4.53	4.99	4.80	5.00	4.76	4.96	4.81
4f (7)	7.00	7.00	7.00	6.25	6.58	6.58	6.99	6.67	6.91	6.91	6.88	6.56
5g (9)		4.78	9.00	6.31	9.00	6.29	8.90	7.31	9.00	7.36	8.68	7.67
6h (11)				6.88	8.46	8.46	10.15	8.12	8.50	8.50	8.96	8.46
7i (13)						6.18	11.97	9.40	12.00	8.26	10.22	8.95
8j (15)								9.72	11.60	11.60	11.82	9.61
9k (17)										8.62	13.49	9.84
10l (19)												10.12
$(L+1)^2$	16	25	25	36	36	49	49	64	64	81	81	100
Number of dependency relations	0	5	0	8	3	13	2	14	7	21	12	30

Furthermore, the total contribution of an entire shell to the MO energy diagram, $f_{\mathrm{TOT}}(l)$, is simply $\sum_{k=-m}^{+m} f_{\mathrm{TOT}}(\varphi_k(\mathrm{GO}))$ in shell l, which can be no larger than $2l+1$. Table 1 summarizes these total contributions to various specific examples of small fullerene cages, and we will discuss these results in the next section.

In the GO method, the average energy of each shell l has a closed form due to the addition theorem for spherical harmonics (ω_N is the angle between the points (θ_i, ϕ_i) and (θ_j, ϕ_j) with respect to the center of the sphere for the cage C_N):

$$\left\langle E_l(\mathrm{GO})\right\rangle = \alpha + 3\beta \sum_{m=-l}^{l} Y_l^{-m}(\theta_i, \phi_i) Y_l^m(\theta_j, \phi_j) = \alpha + 3\beta P_l(\cos\omega_N) = -3P_l(\cos\omega_N), \tag{13}$$

where $P_l(\cos\omega_N)$ is the Legendre polynomial of degree l [33]. The last equality comes from the Hückel assignments of α and β. This simple formula allows a quick evaluation of which shells will give bonding MOs: $\langle E_l(\mathrm{GO})\rangle < 0$. Figure 3 shows that $\langle E_l(\mathrm{GO})\rangle$ drop monotonically with increasing size of the fullerene cage N: as N increases, the number of bonding MOs will increase. This curve also identifies shells that will be nearly net nonbonding for certain fullerene cages. For example, in C_{36} and C_{50}, respectively, the $l = 4$ (5g) and $l = 5$ (6h) shells have average energies near zero. The graph in figure 3 requires establishing the correlation between N and $\cos\omega_N$, which we determined graphically by numerically solving the equation

$$N\pi = 60\arcsin\left(\frac{\tau}{2\cos(\omega_N/2)}\right) + (3N-60)\arcsin\left(\frac{\sqrt{3}}{2\cos(\omega_N/2)}\right), \tag{14}$$

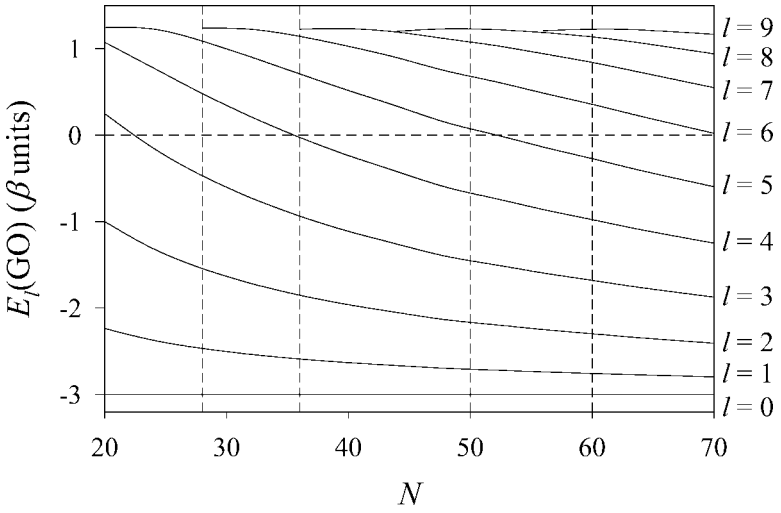

Figure 3. Variations in $\langle E_l(\mathrm{GO})\rangle$ (see equation (13)) with the number of carbon atoms in fullerene cages for different quantum numbers l. Energies less than zero are bonding; energies greater than zero are antibonding.

where τ is the golden mean. Equation (14) arises by dividing the spherical surface into twelve spherical pentagons and $N/2-10$ spherical hexagons involving equal edge lengths. The numerical solution is of equation (14) is

$$\cos\omega_N = 0.80262\big(1-\mathrm{e}^{-0.10049N}\big) + 0.20694\big(1-\mathrm{e}^{-0.01409N}\big). \tag{15}$$

The quantitative application of the GO method does not replace application of the Hückel approach to achieve MO energy values, because both methods require matrix diagonalization. The traditional Hückel method utilizes an adjacency matrix for an orthogonal AO basis as shown in equation (9). However, the GO algorithm does allow rapid assignment of the MOs with respect to the spherical harmonic functions (GOs) and a convenient ("simple") description of the π-MOs in terms of just a few GOs (in many cases, from a single shell), which is difficult to achieve by applying projection operators to the Hückel π-MOs. Furthermore, our results indicate that the shell structure prevails for bonding π-MOs but breaks down somewhat for the antibonding π-MOs in small fullerenes.

5. Computational details

The computer program to perform the GO analysis of the Hückel π-MOs of fullerenes utilized the *eispack* package [34] for matrix diagonalization and was written in FORTRAN. Graphical figures were generated by Sigma Plot Version 7.0 and illustrations of Hückel π-MOs were created using ATOMS Version 5.0 [35].

6. Applications to specific examples

In the remainder of this article, we will examine the π-MO energy diagrams for six different fullerene cages: C_{20}, C_{28}, C_{36}, C_{50}, C_{60} and C_{70}. Justification for choosing these particular cages as examples is as follows: (a) C_{60} and C_{70} are both known structures and well characterized; (b) C_{28} is the fullerene cage with possible cubic symmetry, which forms *endohedral* compounds with various metal atoms; (c) C_{36} is predicted to be a superconductor in the solid state according to recent calculations [36,37]; (d) C_{50} should be a closed shell, stable molecule according to the free-electron model; and (e) C_{20} is the smallest possible fullerene cage.

6.1. C_{20}

"Dodecahedrene" is the first member in the series of possible fullerene-type cages allowed by the restrictions of Euler's theorem: 20 vertices and 12 pentagonal faces (see figure 4). Its idealized structure has point symmetry $\mathcal{I}_h$.

To account for the 20 surface π-MOs in C_{20}, we require 20 GOs that will come from the shells: $1s, 2p, 3d, 4f$, and $5g$. Among these 25 GOs, we obtain five linear dependencies from equation (7) between just the $3d$ and $5g$ shells (this is to be expected from the irreducible representations spanned by the $3d$ shell in the $\mathcal{I}_h$ point group, i.e., h_g, and the $5g$ shell, i.e., $g_g + h_g$). Table 2 summarizes the contribution from each shell of GOs to the Hückel pattern of π-MOs (see also figure 4), which indicates that the π-MOs at $-\beta$ are 84.3% $3d$ and 15.7% $5g$, while the remaining MOs arise from single shells of GOs. Table 2 shows the GO analysis for the overdetermined set ($L = 4$) and the underdetermined set ($L = 3$) and reveals that a shell structure is entirely appropriate for this highly symmetric cage. Furthermore, as figure 4 points out, the energies of the three lowest π-MOs deviate slightly from the spherical free electron model, but fall exactly on the curve expected from equation (13). For the $4f$ and $5g$ shells, the average MO energies agree moderately well with equation (13) but deviate extensively from the free electron expression – the shell structure breaks down for these two sets of functions. From figure 3, the average energy of the $4f$ and $5g$ GOs are greater than zero for C_{20}. This is the first of a general observation that the free electron model breaks down for the antibonding MOs in these fullerene cages. Figure 4 shows that all bonding and nonbonding π-MOs ($E_{\text{Hückel}} \leqslant 0$) fall on the curve from equation (13), but the antibonding π-MOs ($E_{\text{Hückel}} > 0$) deviate extensively from both approximations. Nevertheless, a shell structure to the pattern of occupied π MOs in C_{20} is apparent and is easily assigned from the decomposition of GOs into irreducible representations of the point group $\mathcal{I}_h$.

A neutral C_{20} molecule is predicted to be an open-shell, paramagnetic molecule with two unpaired electrons in the nonbonding "$4f$" HOMO for icosahedral symmetry. *Ab initio* electronic structure calculations show C_{20} is subject to a structural Jahn–Teller distortion [13–18], which breaks the degeneracy of the HOMO with the lowest energy state having the two electrons paired.

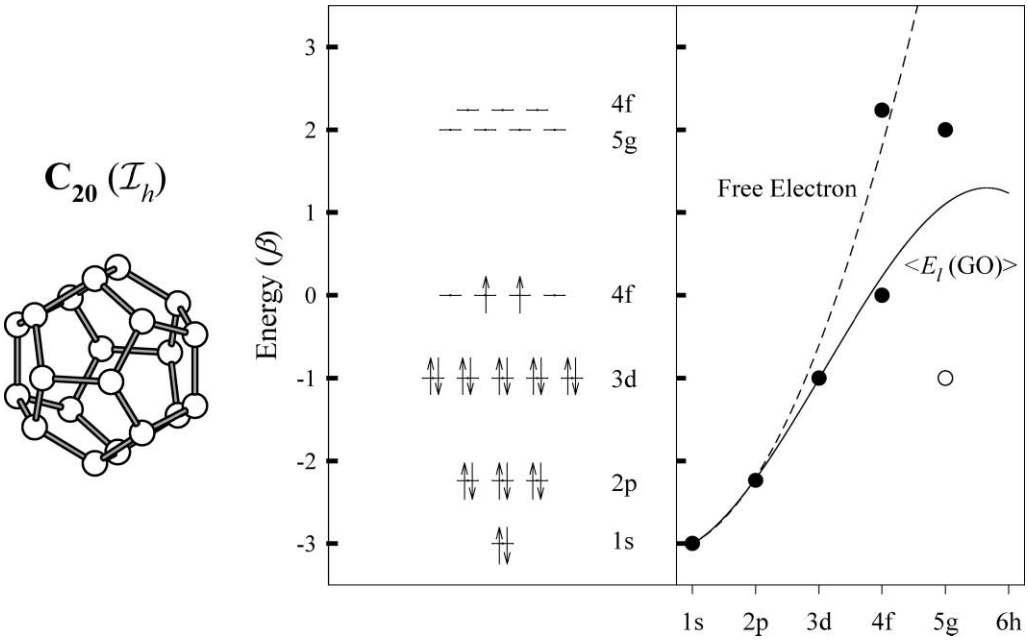

Figure 4. C_{20}: (left) Hückel π-MO energies plotted in units of β (the resonance integral between adjacent carbon atoms); (right) assignment of MO energies to GO shells with fits to the free-electron energies ($E_l^{(\mathrm{FE})}$ in equation (1)) and average GO energies ($\langle E_l(\mathrm{GO})\rangle$ in equation (13)). Filled circles indicate more than 50% contribution of a GO to a π-MO; open circles indicate 33–50% contribution of a GO to a π-MO.

Table 2
Analysis of Hückel π-MO energy values for C_{20} using the GO approach.

$L = 4$		$L = 5$	
$E_{\mathrm{Hückel}}$ (Degeneracy)		$E_{\mathrm{Hückel}}$ (Degeneracy)	
−3.000 (1)	100% s	−3.000 (1)	100% s
−2.236 (3)	100% p	−2.236 (3)	100% p
−1.000 (5)	100% d	−1.000 (5)	84.3% d + 15.7% g
0.000 (4)	100% f	0.000 (4)	100% f
		2.000 (4)	100% g
2.236 (3)	100% f	2.236 (3)	100% f

6.2. C_{28}

As shown in figure 5, this cage molecule is a polyhedron with 12 pentagonal and four hexagonal faces that are arranged in a tetrahedral manner about the molecular center to give point symmetry $\mathcal{T}_d$. This cage is stabilized endohedrally by tetravalent metal atoms such as Ti, Zr, or Hf [38,39]. Formation of endohedral compounds is the probable reason for the presence of strong $[TiC_{28}]^+$, $[ZrC_{28}]^+$, $[HfC_{28}]^+$, and $[UC_{28}]^+$ peaks in the mass spectra of vapors obtained by laser vaporization of the corresponding graphite–metal oxide mixtures [13].

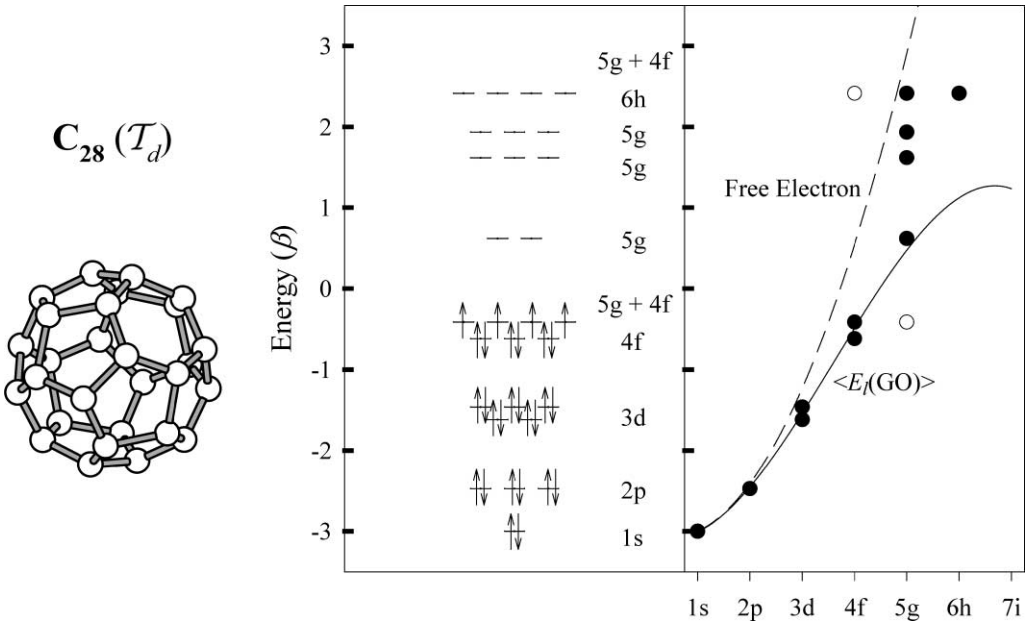

Figure 5. C_{28}: (left) Hückel π-MO energies plotted in units of β (the resonance integral between adjacent carbon atoms); (right) assignment of MO energies to GO shells with fits to the free-electron energies ($E_l^{(\mathrm{FE})}$ in equation (1)) and average GO energies ($\langle E_l(\mathrm{GO})\rangle$ in equation (13)). Filled circles indicate more than 50% contribution of a GO to a π-MO; open circles indicate 33–50% contribution of a GO to a π-MO.

Table 3
Analysis of Hückel π-MO energy values for C_{28} using the GO approach.

$L = 5$		$L = 6$	
$E_{\mathrm{Hückel}}$ (Degeneracy)		$E_{\mathrm{Hückel}}$ (Degeneracy)	
−3.000 (1)	100% s	−3.000 (1)	100% s
−2.473 (3)	98.9% p	−2.473 (3)	98.3% p
−1.618 (2)	99.7% d	−1.618 (2)	92.3% $d + 6.9\%$ h
−1.459 (3)	97.4% d	−1.463 (3)	89.2% $d + 4.5\%$ h
−0.618 (3)	95.7% f	−0.618 (3)	85.6% $f + 11.2\%$ g
−0.414 (1)	44.1% $f + 55.9\%$ g (1)	−0.414 (4)	45.2% $f + 54.8\%$ g (1)
−0.403 (3)	82.2% $f + 17.8\%$ g (3)		78.5% $f + 21.5\%$ g (3)
0.618 (2)	100% g	0.618 (2)	96.4% g
1.618 (3)	99.7% g	1.618 (3)	41.3% $g + 58.7\%$ h
1.938 (3)	16.6% $f + 81.5\%$ g	1.934 (3)	35.3% $g + 58.1\%$ h
2.414 (1)	55.9% $f + 44.1\%$ g (1)	2.414 (4)	94.8% h (3)
			55.9% $f + 44.1\%$ g (1)

To obtain the 28 π-MOs, GOs through the 6h shell are now required. These 36 functions create eight dependency relations, which involve all shells except the 1s shell. Figure 5 illustrates the π-MO energy levels and immediately reveals two acciden-

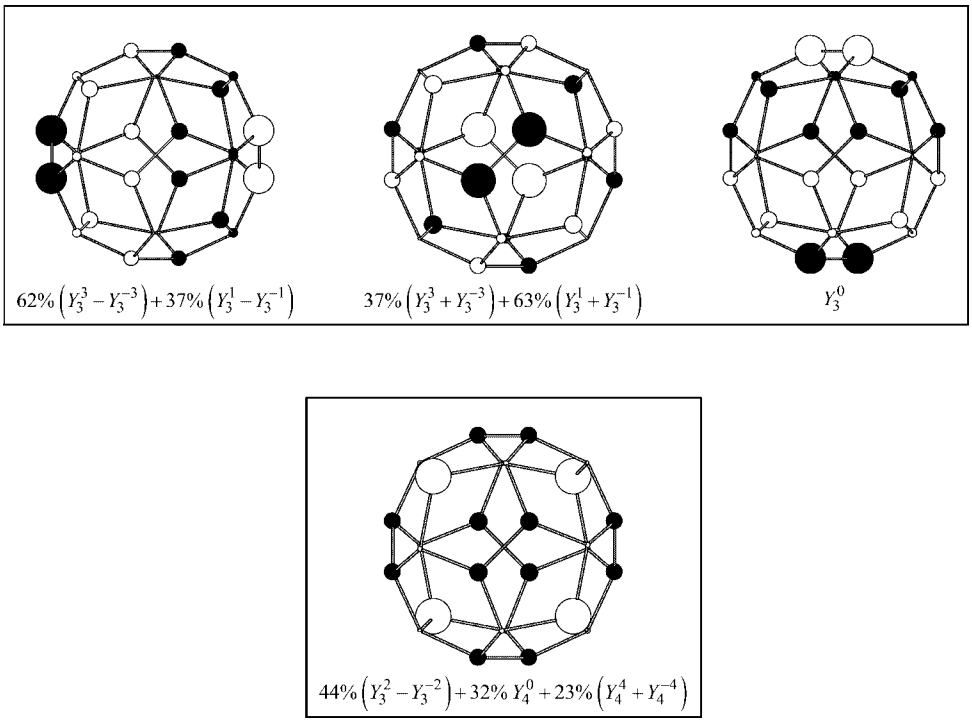

Figure 6. Hückel π-MOs for the accidental degeneracy at the HOMO ($E_{\text{Hückel}} = -0.414\beta$) in C_{28}.

tal, fourfold degeneracies that are not allowed by the tetrahedral point group, namely, the weakly bonding π-MO at $E = -0.414\beta$ and the highest antibonding π-MO at $E = +2.414\beta$. The GO algorithm readily identifies these accidental degeneracies and provides immediate assignment with spherical harmonics (see table 3). The bonding MOs at $E = -0.414\beta$ involve a threefold degenerate set from mostly $4f$ GOs and a nondegenerate combination of $4f$ ($Y_3^2 - Y_3^{-2}$) and $5g$ (Y_4^0 and $Y_4^4 + Y_4^{-4}$) GOs. These π-MOs are illustrated in figure 6 to show their relationship with the GOs: the three nodal surfaces (conical and planar) are clearly apparent for the threefold degenerate set, while the combination of three planar nodes (the xy, xz and yz planes) and four conical nodes gives the "nondegenerate" orbital.

As figure 5 points out, the Hückel energy values of the bonding π-MOs agrees extremely well with equation (13), i.e., the solid line in the right-hand curve. 16 bonding MOs arise mostly from single spherical harmonic shells ($1s, 2p, 3d$ and $4f$), whereas 12 antibonding MOs involve combinations of two higher order shells ($5g$ and $6h$). The energies of these antibonding orbitals fall in the region between the free electron model and the average energy for each GO shell. A closed-shell electronic configuration occurs when four electrons are added to the neutral molecule (i.e., C_{28}^{4-}), which is consistent with the observation that tetravalent metal atoms will stabilize this cage. The valence orbitals of these metals ions such as Ti or Hf, i.e., ns, np, and $(n-1)d$ VAOs, will overlap with the lowest nine occupied π-MOs of the C_{28} cage,

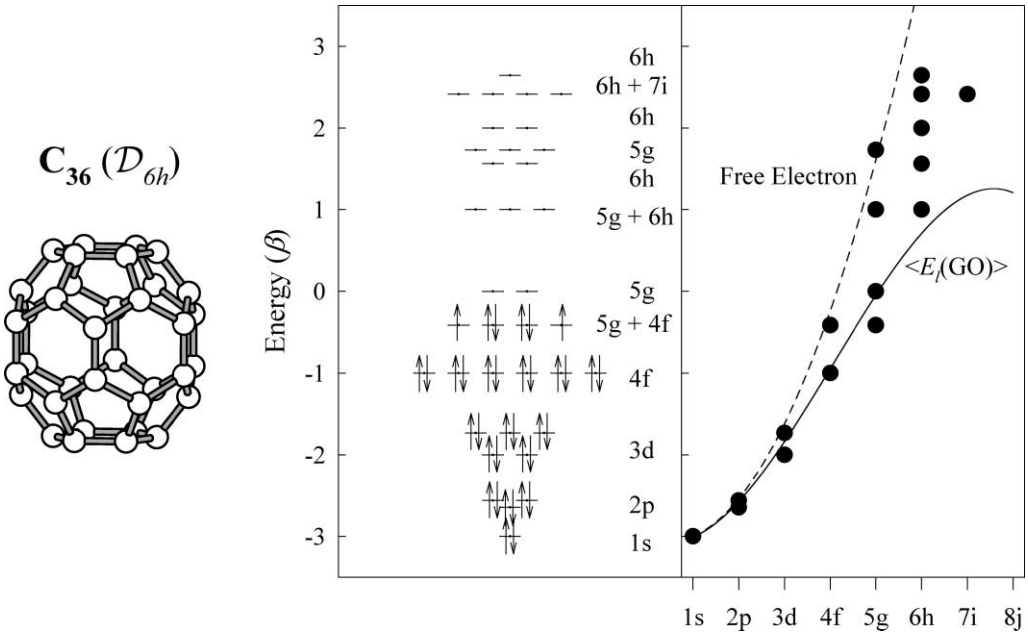

Figure 7. C_{36} ($\mathcal{D}_{6h}$): (left) Hückel π-MO energies plotted in units of β (the resonance integral between adjacent carbon atoms); (right) assignment of MO energies to GO shells with fits to the free-electron energies ($E_l^{(\mathrm{FE})}$ in equation (1)) and average GO energies ($\langle E_l(\mathrm{GO})\rangle$ in equation (13)).

and the extra four electrons will occupy the $4f$ shell of generated MOs to give a closed shell, diamagnetic molecule.

6.3. C_{36}

This fullerene cage is attracting recent excitement due to theoretical calculations suggesting that it may be a superconductor in the solid state [36,37]. The solid-state structure of the cage is predicted to have hexagonal symmetry, point symmetry $\mathcal{D}_{6h}$: the eight hexagons are separated into a waist of six hexagons with the two remaining hexagons at the top and bottom that are surrounded by six pentagons each (figure 7) [8].

Although the dimension of the basis set of GOs through the 6*h* shell is 36, there are three dependency relations so that we must include the 7*i* shell as well. We can see this from the centrosymmetric point group: the 36 π-MOs must contain 18 symmetric and 18 antisymmetric MOs with respect to inversion. The Hückel π-MO energies show a shell structure clearly for the bonding MOs and there are six accidental degeneracies: the point group $\mathcal{D}_{6h}$ only allows doubly degenerate orbitals. Among these accidental degeneracies the sixfold and fourfold orbitals at $-\beta$ and -0.414β, respectively, would be occupied in the neutral C_{36} cage. GO analysis indicates that the sixfold degeneracy arises entirely from the $4f$ shell (i.e., *ungerade* orbitals), whereas one of the fourfold degenerate orbitals derives from the $4f$ shell while the remaining three derive from the $5g$ shell. Therefore, three of these π-MOs are *gerade*, one is *ungerade* (see figure 8). Of

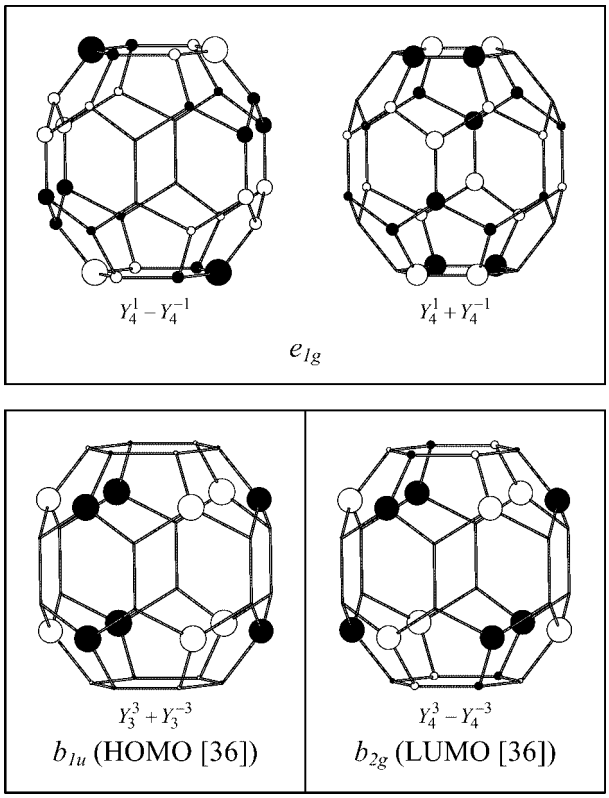

Figure 8. Hückel π-MOs for the accidental degeneracy at the HOMO ($E_{\text{Hückel}} = -0.414\beta$) in C_{36} ($\mathcal{D}_{6h}$).

course, the degeneracies are related to the group of the specific (approximate) Hückel adjacency graph for the structure. These degeneracies will break when modifications are made to the resonance integrals (β_{ij}) to reflect the actual C–C distances in the cage. The Hückel π-MOs for this hexagonal cage agree very well with the results of LDA calculations on $\mathcal{D}_{6h}$ C_{36} and the GO analysis is *exactly consistent* with the assignment of these one-electron states to the irreducible representations of $\mathcal{D}_{6h}$ [40]. We continue to see excellent agreement between the energies of bonding and nonbonding π-MOs with the average GO energies calculated from equation (13), and we also see that the antibonding π-MO energies fall in a band between the free electron and averaged GO energies.

Neutral hexagonal C_{36} would have six electrons in the MO at $E_{\text{Hückel}} = -0.414\beta$ (a mixture of $4f$ and $5g$ shells) and be six electrons short of filling all bonding and nonbonding orbitals ($E_{\text{Hückel}} \leqslant 0$). Therefore, possible closed shell or half-shell configurations arise from C_{36}^{2-}, C_{36}^{4-} (half-shell) and C_{36}^{6-} (note: LDA calculations reveal a diamagnetic configuration for hexagonal C_{36} the accidentally fourfold degenerate level in the Hückel model is split into occupied double degenerate and nondegenerate orbitals and one unoccupied nondegenerate orbital [40]).

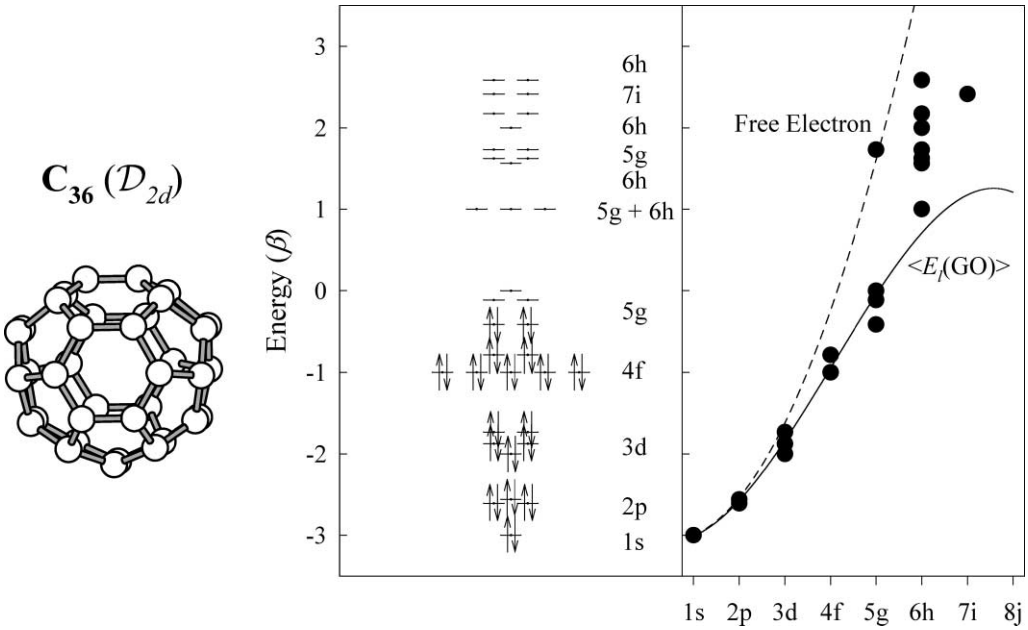

Figure 9. C_{36} ($\mathcal{D}_{2d}$): (left) Hückel π-MO energies plotted in units of β (the resonance integral between adjacent carbon atoms); (right) assignment of MO energies to GO shells with fits to the free-electron energies ($E_l^{(\mathrm{FE})}$ in equation (1)) and average GO energies ($\langle E_l(\mathrm{GO})\rangle$ in equation (13)).

Accurate quantum mechanical calculations suggest that the neutral C_{36} cage in the gas phase may adopt a different structure with point group $\mathcal{D}_{2d}$ (see figure 9), because the calculated cohesive energy and electronic properties are similar to the hexagonal structure [9–11,40]. In this cage, two sets of four hexagons, fused along opposite edges, link together to create 12 pentagonal faces. The Hückel energies again show the expected shell structure and lie between the two spherical models, but there is a clearer (albeit small) separation between the $4f$ and $5g$ shells than in the hexagonal C_{36} cage. The GO calculation of π-MOs requires including the $7i$ shell because the 36 functions generated from shells through the $6h$ spherical harmonics create two dependencies (see table 1; note the different number of dependency relations for this cage versus the hexagonal isomer). Nevertheless, neutral C_{36} in this structure is also six electrons short of filling all bonding and nonbonding MOs, but this neutral molecule would give rise to a diamagnetic molecule with two of the $5g$ GOs filled.

6.4. C_{50}

This hypothetical cage molecule contains 15 hexagons and 12 pentagons and shows fivefold symmetry, point group $\mathcal{D}_{5h}$ (see figure 10). According to the free-electron model, 50 π-electrons would completely fill the $1s$, $2p$, $3d$, $4f$, and $5g$ shells and give a stable, diamagnetic molecule. According to figure 10, the assignment of Hückel π-MO energies in the bonding region ($E_{\mathrm{Hückel}} < 0$) to GOs demonstrates a clear shell

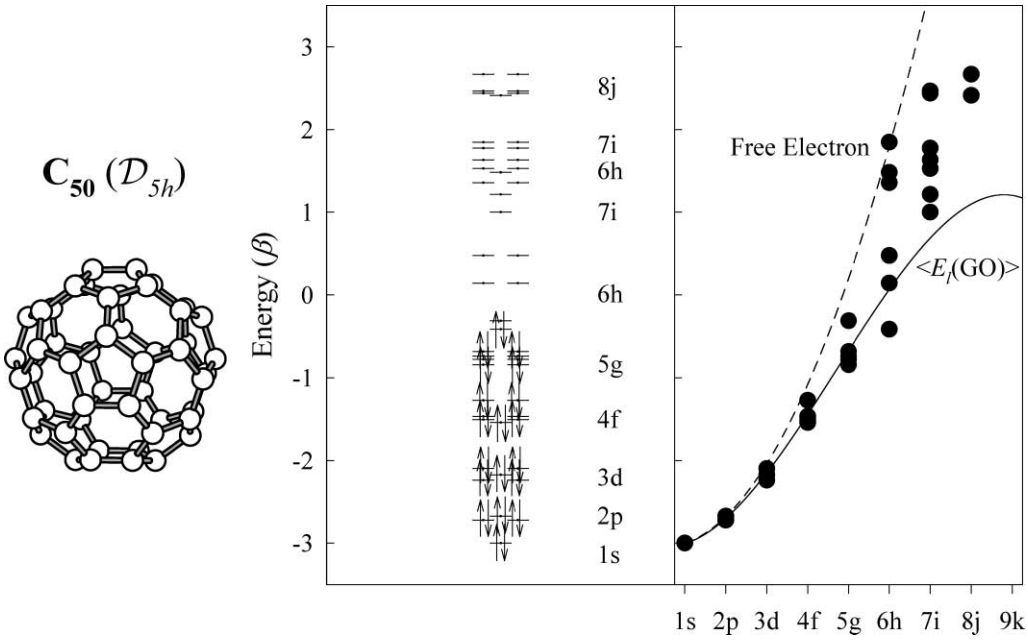

Figure 10. C_{50}: (left) Hückel π-MO energies plotted in units of β (the resonance integral between adjacent carbon atoms); (right) assignment of MO energies to GO shells with fits to the free-electron energies ($E_l^{(\mathrm{FE})}$ in equation (1)) and average GO energies ($\langle E_l(\mathrm{GO})\rangle$ in equation (13)).

structure through the $4f$ shell, but the weakly bonding MOs arise from both the $5g$ and $6h$ shells. Twenty-six π-MOs are bonding or nonbonding, which means that this 50-atom cluster optimizes bonding at 52 π-electrons rather than for the neutral cage, i.e., C_{50}^{2-} should be the stable entity.

6.5. C_{60}

Buckminsterfullerene has 12 pentagonal and 30 hexagonal faces arranged to give icosahedral point symmetry $\mathcal{I}_h$. Figure 11 illustrates its structure as well as its pattern of Hückel π-MO energies and their assignment to the various GOs. Table 4 also lists the sequence of energies calculated by the GO method. The agreement between the two approaches is excellent due to the nearly spherical nature of the soccer ball structure. In particular, the GO approach allows rapid analysis of all occupied and the lowest-lying unoccupied MOs (see table 4). The sixty π-MOs require GOs up to and including the $9k$ shell ($l = 8$; there are 7 dependency relations among the 64 GOs through the $8j$ shell, which does not create a complete description of the 60 π-MOs). The occupied π-MOs readily show a shell structure along the series $1s$, $2p$, $3d$, $4f$, and $5g$. The HOMO and the LUMO in C_{60} are, respectively, fivefold and threefold degenerate levels that are derived from the $6h$ GOs. There is also another threefold degenerate level slightly above the LUMO which comes from the $7i$ shell of GOs rather than the $6h$ GO shell. There are 30 bonding MOs (25 from $1s$ through $5g$ GO shells plus 5 from

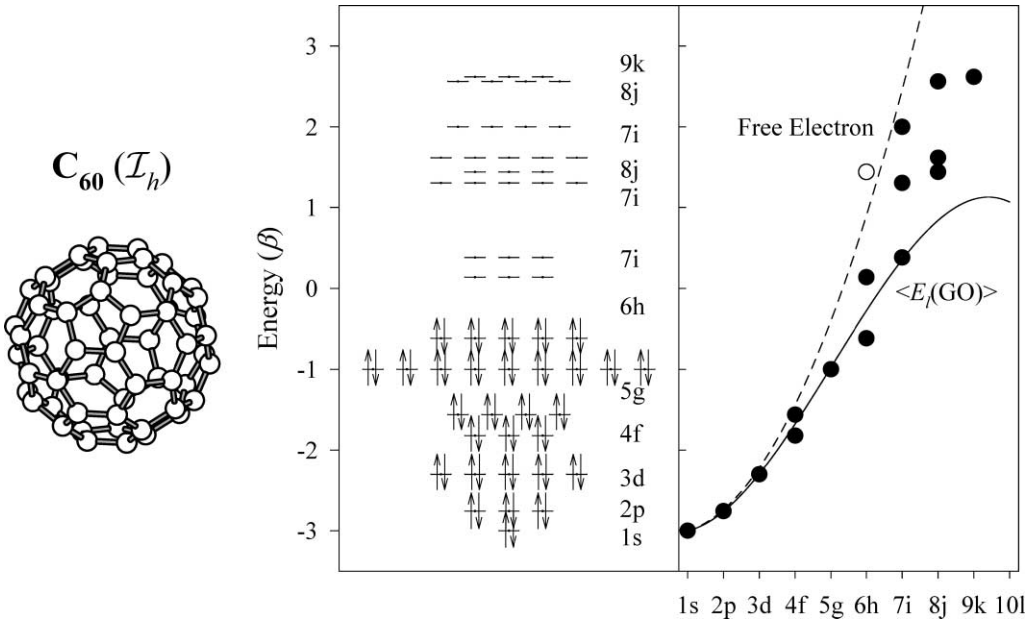

Figure 11. C_{60}: (left) Hückel π-MO energies plotted in units of β (the resonance integral between adjacent carbon atoms); (right) assignment of MO energies to GO shells with fits to the free-electron energies ($E_l^{(\mathrm{FE})}$ in equation (1)) and average GO energies ($\langle E_l(\mathrm{GO})\rangle$ in equation (13)).

Table 4
Analysis of Hückel π-MO energy values for C_{60} using the GO approach.

$L = 7$		$L = 8$	
$E_{\mathrm{Hückel}}$ (Degeneracy)		$E_{\mathrm{Hückel}}$ (Degeneracy)	
−3.000 (1)	99.9% s	−3.000 (1)	99.9% s
−2.757 (3)	99.6% p	−2.757 (3)	99.6% p
−2.303 (5)	94.6% d	−2.303 (5)	94.6% d
−1.820 (3)	96.6% f	−1.820 (3)	96.6% f
−1.562 (4)	93.6% f	−1.562 (4)	93.6% f
−1.000 (9)	90.2% $g + 9.8\%$ i	−1.000 (9)	78.7% $g + 15.0\%$ i
−0.618 (5)	99.3% h	−0.618 (5)	99.3% h
0.139 (3)	66.9% $h + 32.5\%$ j	0.139 (3)	66.9% $h + 32.5\%$ j
0.382 (3)	99.9% i	0.382 (3)	99.9% i
1.303 (5)	95.7% i	1.303 (5)	64.1% $i + 34.1\%$ k
1.438 (3)	48.9% $h + 50.9\%$ j	1.438 (3)	48.9% $h + 50.9\%$ j
1.618 (5)	99.3% j	1.618 (5)	99.3% j
2.000 (4)	20.6% $g + 79.4\%$ i	2.000 (4)	12.3% $i + 84.6\%$ k
2.562 (4)	94.3% j	2.562 (4)	94.3% j
		2.618 (3)	100% k

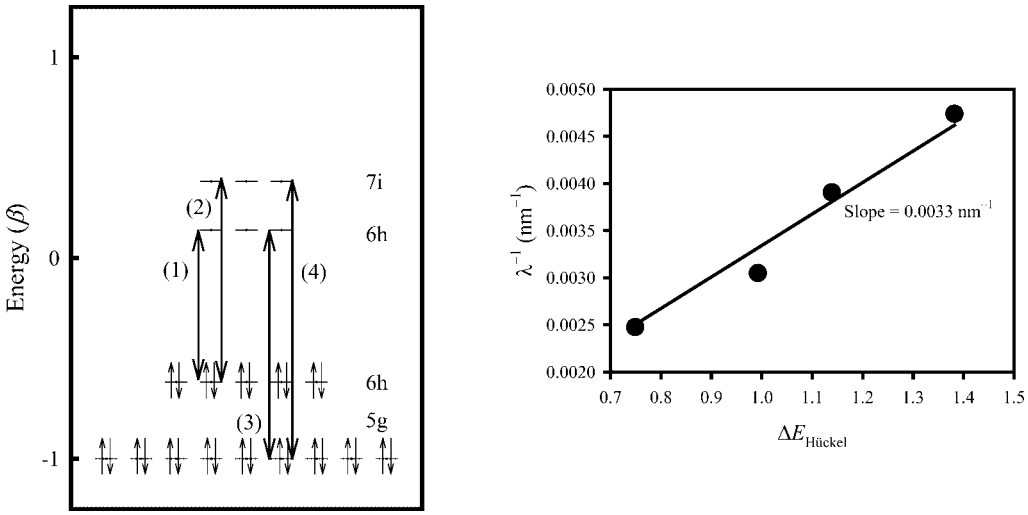

Figure 12. (Left) Hückel π-MO energies for C_{60} near the HOMO and LUMO with GO assignments and electronic excitations noted. (Right) Linear regression fit between $\Delta E_{\text{Hückel}}$ and λ^{-1} (nm^{-1}) for the lowest four assigned excitations in C_{60} [44].

the 6h GO shell), which are completely filled for C_{60}. With 60 valence electrons assigned to these surface π-MOs, the fivefold degenerate HOMO is completely occupied. Therefore, the degeneracy of the 6h shell is broken by the symmetry of the molecule in such a way as to give a closed shell electronic configuration. Furthermore, there are two low-lying LUMOs, which can act as electron acceptors (1c). Therefore, buckminsterfullerene readily forms anionic species, and due to the large size of the C_{60} cage, it can accommodate quite large negative charges [41]. C_{60} also reacts with alkali metals to give metallic products; K_3C_{60} becomes superconducting at 19.3 K [42], while K_6C_{60} is semiconducting [43].

The GO approach is very effective to assign the observed electronic transitions in C_{60}. The UV-visible spectrum [44] reveals four transitions (nm): 404 (weak), 328 (strong), 256 (strong), 211 (medium). Figure 12 illustrates an expansion of the pattern of Hückel π-MO energies, labeled according to their dominant GOs, and four excitations from occupied to unoccupied orbitals. With respect to the GO assignment, the four excitations according to increasing energy are: $(6h) \rightarrow (6h) < (6h) \rightarrow (7i) < (5g) \rightarrow (6h) < (5g) \rightarrow (7i)$. Figure 12 also illustrates a fit between the observed wavelengths and the calculated $\Delta E_{\text{Hückel}}$ values, which is nicely linear. The slope gives an estimate of the resonance integral between two adjacent π orbitals at about 4.1 eV ($\beta = (\text{slope}) \cdot hc$). Furthermore, according to selection rules [45] for electronic excitations, the strongest intensities would be associated with transitions that show $\Delta l = 1$, i.e., $(6h) \rightarrow (7i)$ and $(5g) \rightarrow (6h)$, which agrees with observation. Therefore, the GO approach successfully assigns electronic transitions and the diamagnetic property of C_{60}.

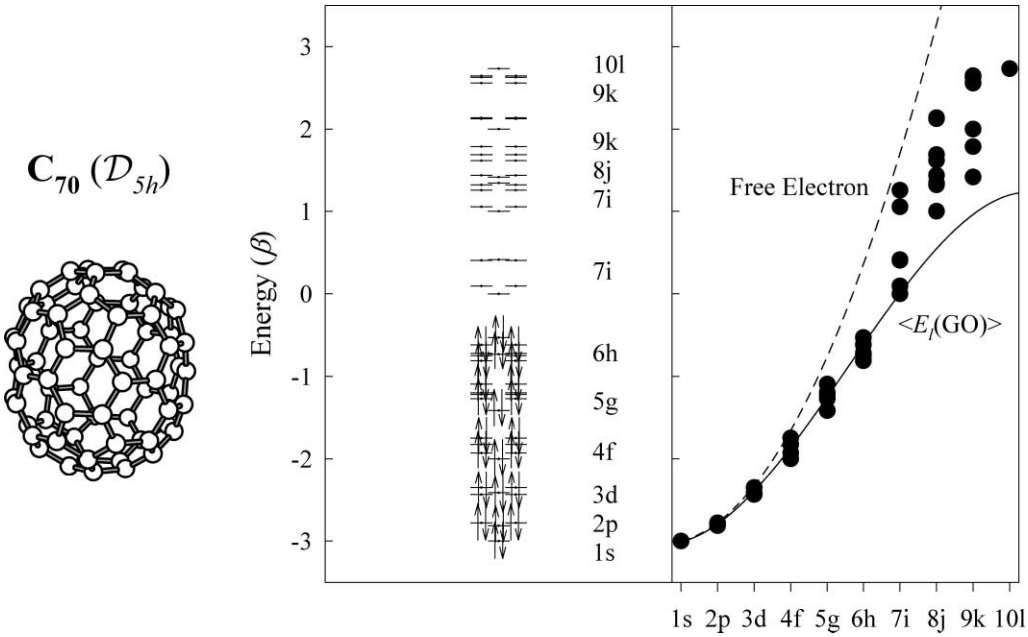

Figure 13. C_{70}: (left) Hückel π-MO energies plotted in units of β (the resonance integral between adjacent carbon atoms); (right) assignment of MO energies to GO shells with fits to the free-electron energies ($E_l^{(\mathrm{FE})}$ in equation (1)) and average GO energies ($\langle E_l(\mathrm{GO})\rangle$ in equation (13)).

6.6. C_{70}

We conclude our applications with a brief examination of C_{70}, which is the second most abundant carbon cluster extracted from the soot produced by the vaporization of graphite. Fullerene mixtures containing anywhere between 15% and 50% of C_{70} have been reported [13]. We can construct C_{70} by "cutting" C_{60} in half, which creates two bowl-shaped C_{30} units. These two fragments are then pulled apart and twisted 36° with respect to each other. Finally, 10 additional carbon atoms are inserted in the equatorial plane to create a "belt" of five new hexagons. The resulting C_{70} cage has 12 pentagonal and 25 hexagonal faces (see figure 13). According to this construction, C_{70} has cylindrical symmetry, point group $\mathcal{D}_{5h}$, which gives nondegenerate and twofold degenerate MOs, as seen in figure 13.

The GO analysis requires including GOs through the 10l shell: the 81 GOs through the 9k shell give 12 dependency relations. Once again, the shell structure is clearly apparent for the lowest occupied bonding levels generated by the $1s$, $2p$, $3d$, $4f$, and $5g$ GOs. These five shells of GOs account for 25 of the 35 occupied MOs. The 6h GO shell contains the HOMO, and, according to the GO analysis, ten of the 11 6h GOs give bonding MOs. These 10 MOs have been assigned to the first ionization band from the photoelectron spectrum of C_{70} [46] (note: the second ionization band consists of the nine MOs assigned to the $5g$ shell). The HOMO as calculated by this method arises almost exclusively from the Y_5^0 GO; the LUMO is also nondegenerate (although there is

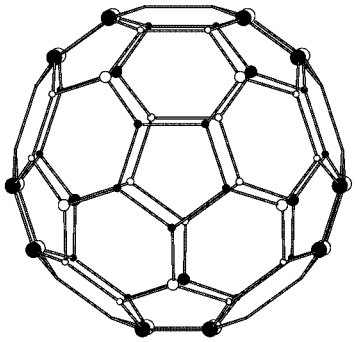

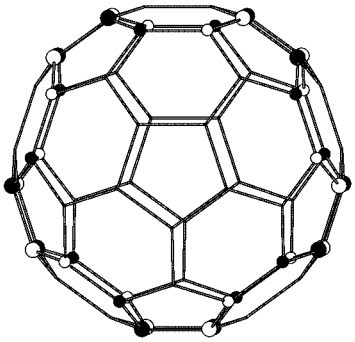

C_{70} HOMO: $Y_5^0\ (a_2'')$ **C_{70} LUMO:** $Y_5^5 - Y_5^{-5}\ (a_1')$

Figure 14. (Left) The HOMO for C_{70} as determined by the GO method along with the nodal planes for the appropriate $6h$ GO; (right) the LUMO for C_{70} as determined by the GO method along with the nodal planes for the appropriate $7i$ GO.

a closely lying double degenerate MO just above) which is from the $7i$ shell ($Y_6^5 - Y_6^{-5}$); see figure 14. According to figure 13, the GO approach is well suited to account for the large HOMO–LUMO energy gap in neutral C_{70} and account for its diamagnetic behavior.

Electronic spectra in the UV and visible have also been reported for C_{70}, and our GO analysis can assist with the analysis. The UV-visible spectrum [47] reveals several transitions ranging from 544 nm to 215 nm. Figure 15 illustrates an expansion of the pattern of Hückel π-MO energies, labeled according to their dominant GOs, and the first three allowed excitations from occupied to unoccupied orbitals. With respect to the GO assignment, all excitations involve $(6h) \rightarrow (7i)$ orbitals. Figure 15 also illustrates a fit between the observed wavelengths and the calculated $\Delta E_{\text{Hückel}}$ values, which is nicely linear for the lower energy transition, but shows poorer fit towards higher energy. The slope gives an estimate of the resonance integral between two adjacent π orbitals at about 4.5 eV ($\beta = (\text{slope}) \cdot hc$), which is consistent with the corresponding fit from C_{60} (see figure 12).

7. Summary

The nearly spherical symmetry of small fullerenes, i.e., C_N for $N \leqslant 70$, also provides a means to compare different models of electronic structure: a free electron model in which electronic energy is entirely kinetic energy versus a "tight-binding" model in which electrons are closely bound to individual atoms but allowed to "delocalize" throughout the molecule via atomic orbital overlaps. We have taken the seven structural examples presented in this paper, and compared the coefficient in the free-electron expression for the orbital energies, $E_l = (A/R^2)l(l+1)$ (see equation (3)), with the three lowest shells of MOs (i.e., the $1s, 2p$ and $3d$ shells). Since the Hückel

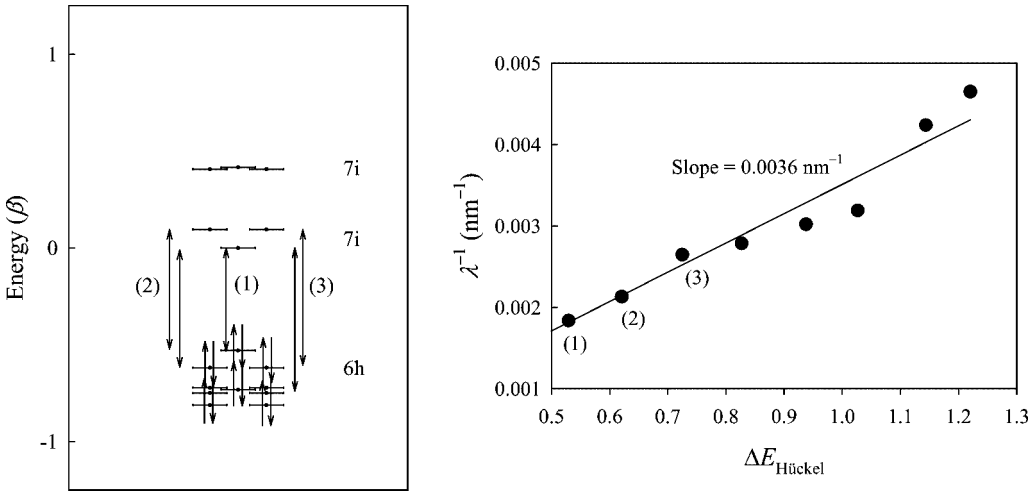

Figure 15. (Left) Hückel π-MO energies for C_{70} near the HOMO and LUMO with GO assignments and electronic excitations noted. (Right) Linear regression fit between $\Delta E_{\text{Hückel}}$ and λ^{-1} (nm^{-1}) for the lowest three assigned excitations in C_{70} [47].

energies are quoted in units of β, which is the strength of each C–C π-type interaction in the cage, the fit gave $\beta = 2.4$ eV (an appropriate value for this type of interaction in aromatic hydrocarbons). Note that this value is smaller than 4.1–4.5 eV estimated from the excitation spectra of C_{60} and C_{70}.

The generator atomic orbital approach allows one to make a quick determination of the qualitative molecular orbitals for many molecules. This method is particularly advantageous for the construction and analysis of Hückel energy level diagrams of fullerene-type molecules and corresponding molecular ions through simple computations, since the distribution of carbon atoms is largely on a single spherical shell. The GO approach also demonstrates that simple spherical models allows a rapid nearly quantitative assessment of the bonding and nonbonding π-MOs in these cage molecules, but cannot reproduce the entire energy diagram in the antibonding region because the set of spherical harmonics is not a set of mutually orthogonal functions. Nevertheless, these antibonding π-MOs do fall in a band of energy values intermediate between the free electron model and the average GO energies.

Since the fullerene cages are nearly spherical, the simplest application of the GO method would predict stable π-electron counts for fullerene molecules to be 32 ($l = 4$), 50 ($l = 5$), 72 ($l = 6$), 98 ($l = 7$), $\ldots$, $2l^2$, $\ldots$, i.e., closed shells of GOs where large HOMO–LUMO gaps may appear. However, C_{60} and C_{70} with 60 and 70 π-electrons, respectively, are the major products of laser vaporization experiments. Therefore, orbital overlap significantly breaks up the degeneracies of each shell. The GO approach reproduces the nodal characteristics of the MOs for these fullerene cages, and provides a rapid assessment of how these nodal characteristics break up the energies of the shells to account for the stability of C_{60} and C_{70} by completely occupying all bonding MOs. The GO approach also allows a rapid assessment of how these gaps occur in

C_{60} and C_{70}, and can even lead to an assignment of the UV-visible excitation spectrum in C_{60}.

Acknowledgements

The authors wish to thank Klaus Ruedenberg for several useful discussions regarding canonical orthogonalization.

References

[1] H.W. Kroto, J.R. Heath, S.C. O'Brien, R.F. Curl and R.E. Smalley, Nature 318 (1985) 162.
[2] R.F. Civil and R.E. Smalley, Scientific American 54 (1991).
[3] Acct. Chem. Res. 25 (1992).
[4] K. Hedberg, L. Hedberg, D.S. Bethune, C.A. Brown, H. Dorn, R.D. Johnson and M. de Vries, Science 254 (1991) 410.
[5] F.J. Rioux, J. Chem. Educ. 71 (1994) 464.
[6] R. Taylor, J.P. Hare, A.K. Abdul-Sada and H.W. Kroto, J. Chem. Soc. Chem. Commun. (1990) 1423.
[7] K. Hedberg, L. Hedberg, M. Bühl, D.S. Bethune, C.A. Brown and R.D. Johnson, J. Am. Chem. Soc. 119 (1997) 5314.
[8] C. Piskotti, J. Yarger and A. Zettl, Nature (London) 393 (1998) 771.
[9] B.L. Zhang, C.Z. Wang, K.M. Ho, C.H. Xu and C.T. Chan, J. Chem. Phys. 97 (1992) 5007.
[10] B.L. Zhang, C.Z. Wang, K.M. Ho, C.H. Xu and C.T. Chan, J. Chem. Phys. 98 (1993) 3095.
[11] A.A. Kuzubov, P.V. Avramov, A.A. Zakharov, S.G. Ovchinnikov, S.A. Varganov and F.N. Tomilin, Zh. Neorg. Khim. 46(3) (2001) 467–473.
[12] H.M.S. Coxeter, *Regular Polytopes*, 2nd ed. (Macmillan, New York, 1963).
[13] J. Cioslowski, *Electronic Structure Calculations on Fullerenes and Their Derivatives* (Oxford University Press, New York, 1995).
[14] R.C. Haddon, L.E. Brus and K. Raghavachari, Chem. Phys. Lett. 125 (1986) 459.
[15] P.W. Fowler and J. Woolrich, Chem. Phys. Lett. 127 (1986) 78.
[16] J.R. Dias, J. Chem. Educ. 66 (1989) 1012.
[17] S. Saito and A. Oshiyama, Phys. Rev. Lett. 66 (1991) 2637.
[18] D.E. Manolopoulos, J.C. May and S.E. Down, Chem. Phys. Lett. 181 (1991) 105.
[19] D.B. Redmond, C.M. Quinn and P.W. Fowler, J. Math. Chem. 23 (1998) 263 and references therein.
[20] P.W. Fowler and K.M. Rogers, J. Chem. Soc. Faraday Trans. 94 (1998) 1019.
[21] P.W. Fowler and J.I. Steer, J. Chem. Soc. Chem. Commun. (1987) 1403.
[22] T.A. Albright, J.K. Burdett and M.-H. Whangbo, *Orbital Interactions in Chemistry* (Wiley, New York, 1985).
[23] J.G. Verkade, *A Pictorial Approach to Molecular Bonding and Vibrations*, 2nd ed. (Springer-Verlag, New York, 1997) and references therein.
[24] G.J. Miller and J.G. Verkade, J. Chem. Educ. 76 (1999) 428.
[25] J.G. Verkade, J. Chem. Educ. 68 (1991) 739.
[26] J.K. Burdett, *Chemical Bonding in Solids* (Oxford University Press, New York, 1995).
[27] R.C. Haddon, J. Am. Chem. Soc. 119 (1997) 1797.
[28] D.W. Ball, J. Chem. Educ. 71 (1994) 463.
[29] G. Wannier, Phys. Rev. 64 (1943) 359.
[30] T.C. Chen, J. Chem. Phys. 29 (1958) 347.
[31] R. Hoffman and M. Gouterman, J. Chem. Phys. 36 (1962) 2189.
[32] J. Ivanic and K. Ruedenberg, J. Phys. Chem. 100 (1996) 6342.

[33] D.M. Mingos and D.J. Wales, *Introduction to Cluster Chemistry* (Prentice Hall, Englewood Cliffs, NJ, 1990).
[34] B.S. Garbow, *Eispack* matrix diagonalization package, Applied Mathematics Division, Argonne National Laboratory.
[35] E. Dowty, ATOMS Version 5.0.
[36] M. Côté, J.C. Grossman, M.L. Cohen and S.G. Louie, Phys. Rev. Lett. 81 (1998) 697.
[37] J.C. Grossman, M. Côté, S.G. Louie and M.L. Cohen, Chem. Phys. Lett. 284 (1998) 344.
[38] T. Guo, M.D. Diener, Y. Chai, M.J. Alford, R.E. Haufler, S.M. McClure, T. Ohno, J.H. Weaver, G.E. Scusceria and R.E. Smalley, Science 257 (1992) 1661.
[39] N. Rösch, O.D. Häberlen and B.I. Dunlap, Angew. Chem. 105 (1993) 78; Angew. Chem. Int. Ed. Engl. 32 (1993) 108.
[40] G.K. Gueorguiev and J.M. Pacheco, J. Chem. Phys. 114 (2001) 6068.
[41] P.D.W. Boyd, P. Bhyrappa, P. Paul, J. Stinchcombe, R.D. Bolskar, Y. Sun and C.A. Reed, J. Am. Chem. Soc. 117 (1995) 2907.
[42] P.W. Stephens, L. Mihaly, P.L. Lee, R.L. Whetten, S.-M. Huang, R. Kaner, F. Diederich and K. Holczer, Nature 351 (1991) 632.
[43] O. Zhou, J.E. Fischer, N. Coustel, S. Kycia, O. Zhu, A.R. McGhie, W.J. Romanow, J.P. McCauley Jr., A.B. Smith III and D.E. Cox, Nature 351 (1991) 462.
[44] J.P. Hare, H.W. Kroto and R. Taylor, Chem. Phys. Lett. 177 (1991) 394.
[45] I.N. Levine, *Quantum Chemistry*, 2nd ed. (Allyn and Bacon, Boston, 1974) p. 98.
[46] D.E. Lichtenberger, M.E. Rempe and S.B. Gogosha, Chem. Phys. Lett. 198 (1992) 454.
[47] R.L. Whetten, M.M. Alvarez, S.J. Anz, K.E. Schriver, R.D. Beck, F.N. Diederich, Y. Rubin, R. Ettl, C.S. Foote, A.P. Darmanyan and J.W. Arbogast, Mat. Res. Soc. Symp. Proc. 206 (1991) 639.